International Journal of ChemTech Research
CODEN (USA): IJCRGG, ISSN: 0974-4290, ISSN(Online):2455-9555
Vol.10 No.5, pp 178-189, 2017

Growth and Characterization of Semi-Organic Third Order NLO Material: Bisglycine Barium Dichloride Single Crystals

L. Gobinathan[1], K. Boopathy[2]

[1]Department of Physics, VSA Group of Institutions, Salem, TamilNadu., India
[2]Department of Physics., Govt.Engineering College, Dharmapuri, TamilNadu., India

Abstract : Optical quality single crystals of bisglycine barium dichloride were grown by slow evaporation solution growth technique. The cell parameters of the grown crystals were estimated by single crystal X – ray diffraction analysis. The grown crystals were characterized by powder X – ray diffraction and Fourier transforms infrared spectral analysis. The range and percentage of optical transmission was ascertained by recording UV – Vis – NIR transmittance spectral analysis. The mechanical strength of grown crystal was estimated by using Vicker's microhardness tester. The dielectric response of the grown crystal was investigated in the frequency range of 50 Hz – 2 MHz. Thermogravimetric and differential thermal analysis were carried out to investigate the thermal properties of grown crystal. The third order nonlinear optical properties were studied in detail by Z – scan technique with He-Ne laser radiation of wavelength at 632.8 nm and the corresponding nonlinear refractive index, absorption coefficient and optical susceptibility were calculated.
Keywords: Synthesis. Crystal growth. X – ray diffraction. Z – Scan studies.

1. Introduction

Nonlinear optical materials are expected to play a major role in the technology of photonics including optical information processing, optical modulation, optical switching, optical logic, frequency shifting, optical data storage for the developing technologies in telecommunications and signal processing [1, 2]. Amino acids are interesting materials formed by weak van der Waals hydrogen bonds; they contain a proton donor carboxyl acid (COO^-) group and the proton acceptor amino (NH_3^+) group. Due to this dipolar nature, amino acids have physical properties that make them ideal candidates for NLO applications. It also offers an opportunity for theoretical modeling and synthetic flexibility to design and produce novel materials [3]. Glycine is the simplest amino acid and exists in three polymorphic forms α, β and γ. Both α and β forms crystallize in centrosymmetric space group $P2_1/c$, ruling out the possibility of optical second harmonic generation [4]. But γ – glycine crystallizes in noncentrosymmetric space group $P3_1$, making it a possible candidate for NLO applications [5]. The glycine molecule is prochiral, containing two hydrogen atoms at the central carbon atom that are enantiotopic namely; replacement of one of these hydrogen atoms by a different group yields a chiral molecule [6]. Crystal structures of compounds of glycine with halogen or metal halogenides have already been reported. Some of these compounds of glycine with inorganic salts have been studied extensively for their physical properties such as ferroelectricity, thermal and optical behaviour [7–14]. Michel Fleck [15] has reported a comprehensive study on the structural relations between glycine complexes and introduced classification scheme. Narayanan et al. have [16] carried out X - ray single crystal structure solution of bisglycine barium dichloride and reported that it belongs to orthorhombic crystal structure with the space group of Pbcn. Single crystal growth and characterization of glycine barium chloride have been reported for its NLO applications [17

- 19]. In the present work studies on the growth, spectroscopic, optical, mechanical, dielectric, thermal and third harmonic generation efficiency of BGBDC crystals were carried out and presented.

2. Experimental Section

2.1 Synthesis

The BGBDC salt was synthesized by taking glycine and barium chloride (AR grade) in the molar ratio 2:1. Calculated amount of salts were dissolved in double distilled water at room temperature and then the resultant solution was stirred well using temperature controlled magnetic stirrer. The solution was allowed to evaporate at room temperature, which gives white crystalline salt of BGBDC. The purity of the synthesized salt was further increased by repeated recrystallization process. The reaction mechanism of the synthesized BGBDC salt is depicted as below

$$2(CH_2NH_2COOH) + BaCl_2.2H_2O \rightarrow Ba(CH_2NH_2COOH)_2Cl_2.H_2O + H_2O\uparrow$$

2.2 Solubility

The solubility of BGBDC was determined for five different temperatures, i.e., 30 °C, 35 °C, 40 °C, 45 °C and 50 °C. The solubility was determined by dissolving the recrystallized salts in 100 mL of double distilled water in an air tight container maintained at a constant temperature with continuous stirring. After attaining the saturation, the equilibrium concentration of the solute was analyzed gravimetrically. The same process was repeated to determine the solubility at different temperatures. The variation of solubility with different temperature is shown in Fig. 1.

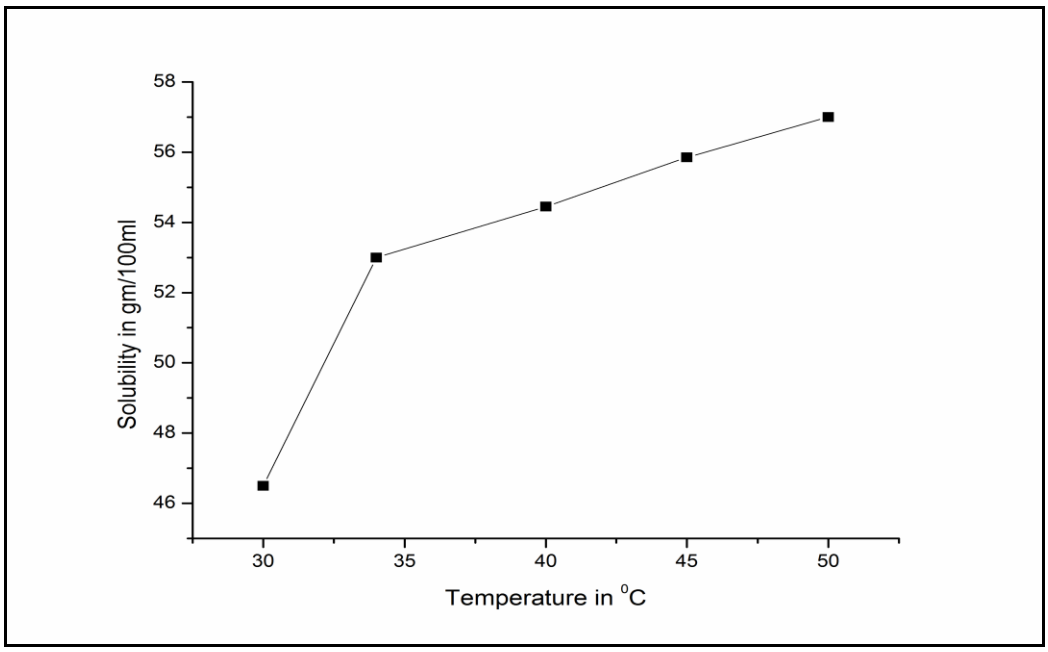

Fig. 1 Solubility curve of BGBDC

2.3 Crystal growth

The purified crystalline salt of BGBDC was dissolved in double distilled water at room temperature to prepare the saturated solution and filtered using Whatmann filter paper. Then the solution was covered with perforated polythene sheet and kept in a dust free atmosphere. The solvent was evaporated slowly at room temperature. After the growth period of 15 days good quality of single crystals were harvested from the mother solution. Optically transparent crystal of BGBDC was grown with the dimensions of 14 × 7 × 6 mm^3 and is shown in Fig. 2.

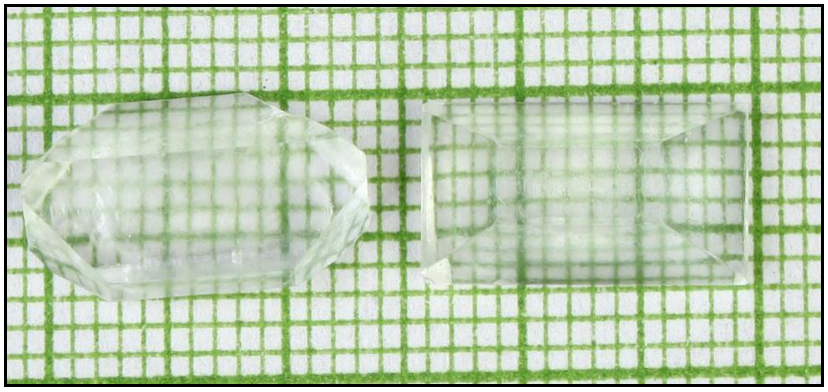

Fig. 2 As grown crystals of BGBDC

3. Result and discussion

3.1 Single crystal X – ray diffraction

The grown crystal was subjected to single crystal X – ray diffraction study at room temperature using Enraf Nonius CAD4 - F single crystal X – ray diffractometer with graphite monochromated Mo Kα (λ= 0.71073 Å) radiation. From the single crystal X – ray diffraction analysis, it is observed that the BGBDC crystal belongs to orthorhombic crystal system with unit cell parameters a = 8.267 (3) Å, b = 9.294 (3) Å, c = 14.829 (2) Å, α, β and γ = 90 °, which is in good agreement with the reported value [16].

3.2 Powder X – ray diffraction

The powder X – ray diffraction pattern was recorded on a REICH SIEFERT X – ray diffractometer using Cu Kα (1.5418 Å) radiation. The sample was scanned over the 2θ range 10 - 80° at a rate of 1°/min. The resulting powder X – ray diffraction pattern is shown in Fig. 3. All the observed reflection lines were indexed using the software AUTOX 93. From the X – ray diffraction patterns, it was observed that the crystallinity of BGBDC crystal is good.

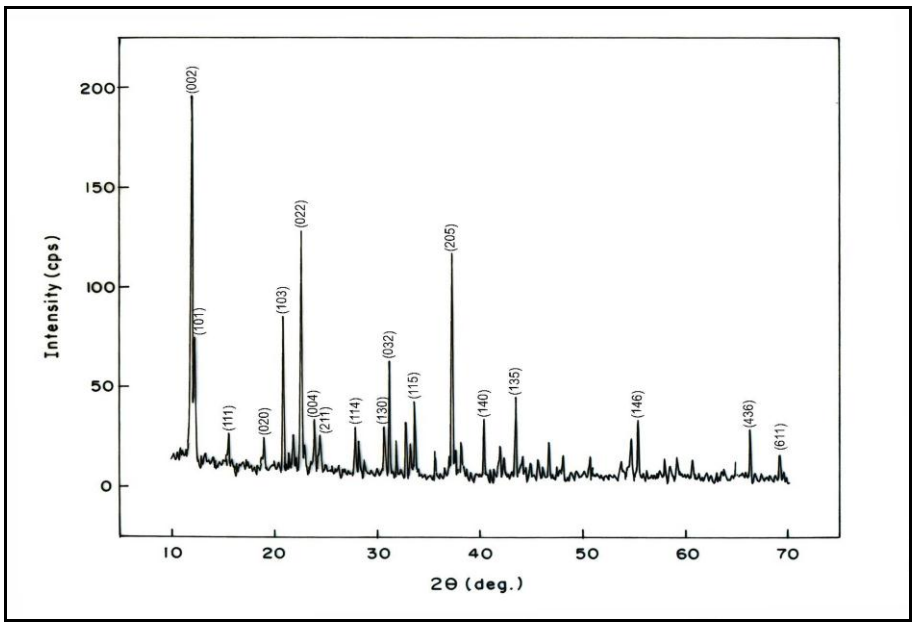

Fig. 3 Powder X – ray diffraction pattern of BGBDC single crystal

3.3 Fourier Transform Infrared (FTIR) spectrum

The FTIR spectral analysis of BGBDC was carried out in the middle infrared region extending from 400 – 4000 cm^{-1} using a Perkin Elmer FTIR spectrometer by the KBr pellet method. The sample was prepared by mixing it with KBr. The recorded FTIR spectrum of BGBDC is shown in Fig. 4. In the higher energy region, there is a broad intense band due to the N – H asymmetric stretching of NH_3^+. The band at 1592 cm^{-1} is attributed to the asymmetric stretching vibration of COO^-. The CH_2 deformation scissoring and wagging vibrations are observed at 1414 and 1332 cm^{-1} respectively. The strong band appearing at 1110 cm^{-1} in the spectrum is assigned to CH_2 rocking vibration. The asymmetric and symmetric C – C – N stretching vibration bands are observed at 1032 and 897 cm^{-1}. The NH_2 rocking vibration appears at 777 cm^{-1}. The COO^- rocking vibration appears as well – resolved sharp peak at 503 cm. The different functional groups are presented in Table 1.

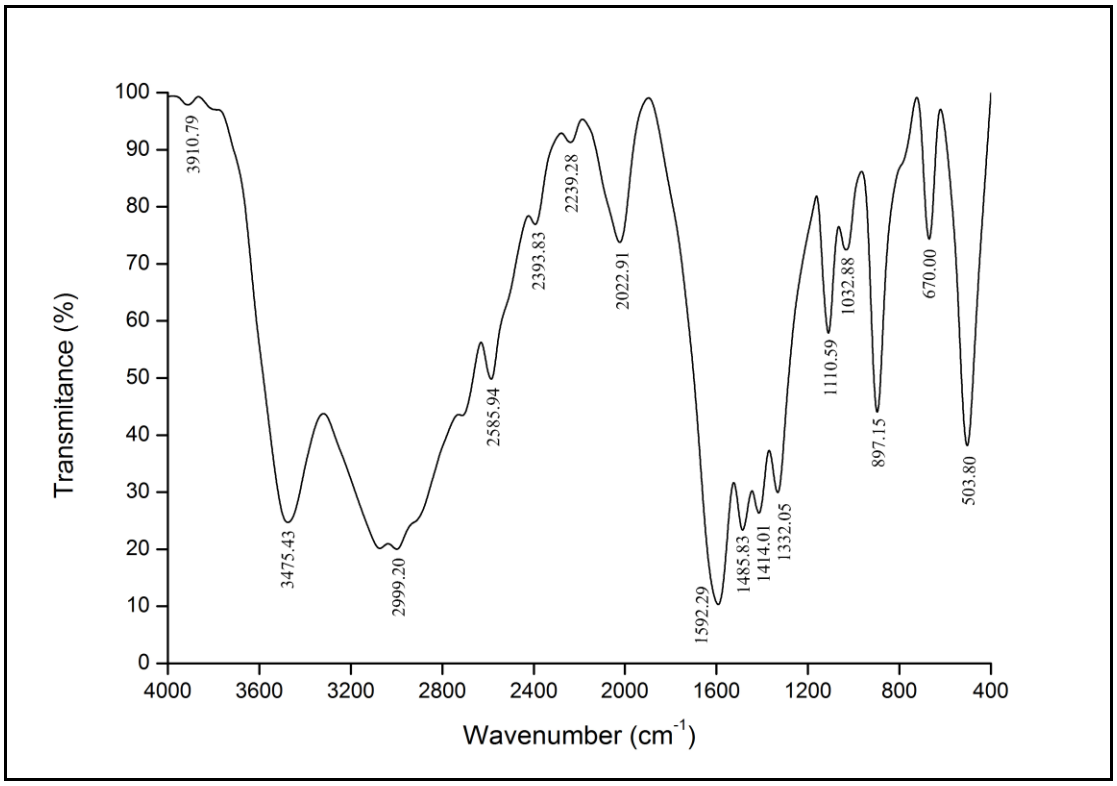

Fig. 4 FTIR spectrum of BGBDC crystal

Table 1 Vibrational frequency assignments

FT – IR	Band Assignments
3910	NH_3 asymmetric stretching
3475	NH_3 symmetric stretching
2999	C – H stretching
1592	COO^- asymmetric stretching
1485	CH_2 bending vibration
1414	CH_2 deformation scissoring
1332	CH_2 wagging vibration
1110	CH_2 rocking vibration
1032	C – C – N asymmetric stretching
897	C – C – N symmetric stretching
777	NH_2 rocking vibration
670	COO^- wagging vibration
503	COO^- rocking vibration

3.4 UV – Vis – NIR spectral analyses

The UV – Vis – NIR spectrum gives information about the structure of the molecule because the absorption of UV and visible light involves promotion of the electron in the σ and π orbitals from the ground state to higher energy state. To determine the transmission range of BGBDC, the optical transmission spectrum was recorded between 190 and 1100 nm using Varian Carry 5E UV – Vis – NIR spectrophotometer. A crystal thickness of 3 mm was used for this study. The recorded UV – Vis – NIR transmittance spectrum is shown in Fig. 5. From the graph, it is evident that the BGBDC crystal has a UV very low cutoff wavelength 220 nm, which is suitable material for nonlinear optical applications.

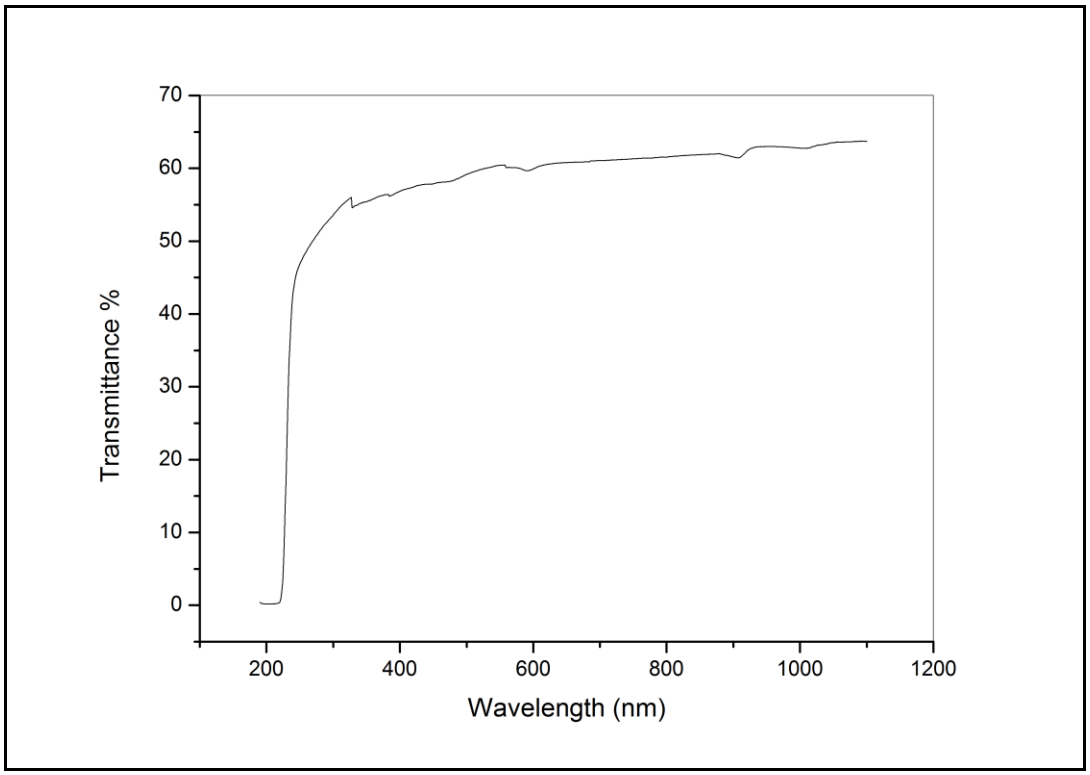

Fig. 5 UV – Vis – NIR transmittance spectrum of BGBDC crystal

3.5 Vicker's microhardness studies

The microhardness measurement was carried out with the load ranging from 25 to 100 g using the Vicker's hardness tester (Shimadzu HMV – 2) fitted with a diamond pyramidal indenter and attached to an incident light microscope. The Vicker's hardness number was calculated using the relation $H_v = 1.8544 (P/d^2)$ kg/mm^2, where P is the indenter load and d is the diagonal length of the indentation impression in mm. Fig. 6 shows the variation of load P versus Vicker's hardness number (H_v). From the graph it is evident that the Vicker's hardness number increases with the applied load P. The hardness value increases upto a load of 100 g. Cracks develop around the indentation mark above the load of 100 g. The work hardening coefficient n was calculated from Meyer's law.

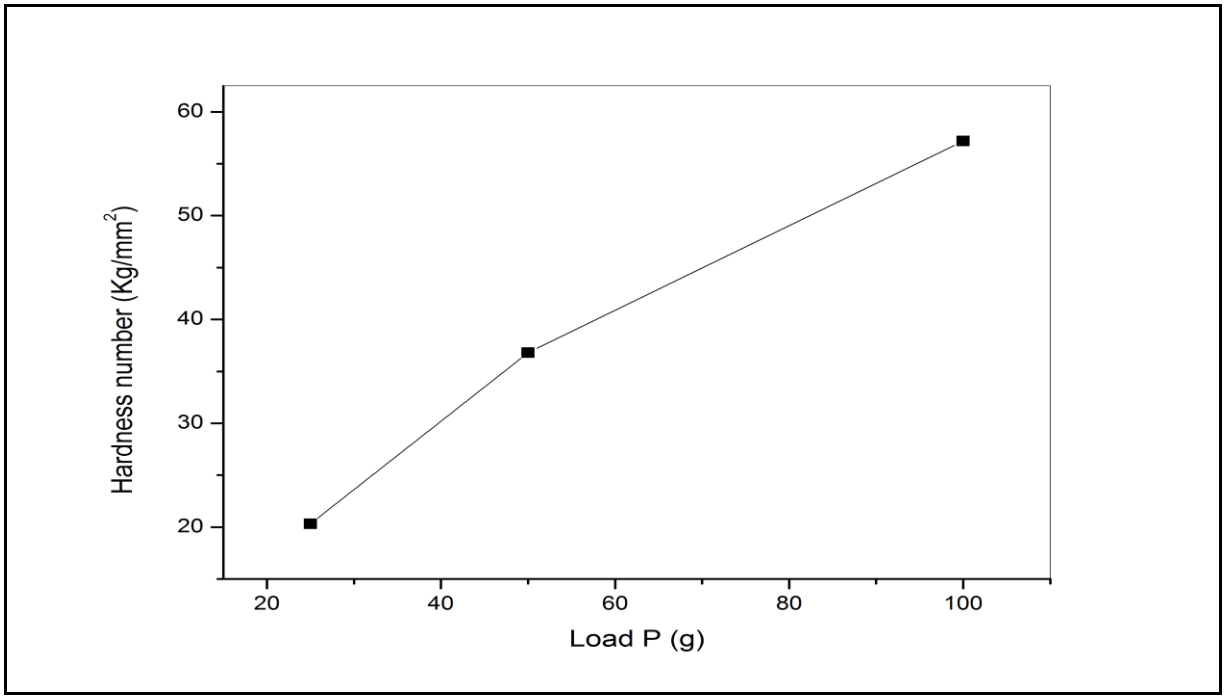

Fig. 6 Hardness vs. load graph of BGBDC crystal

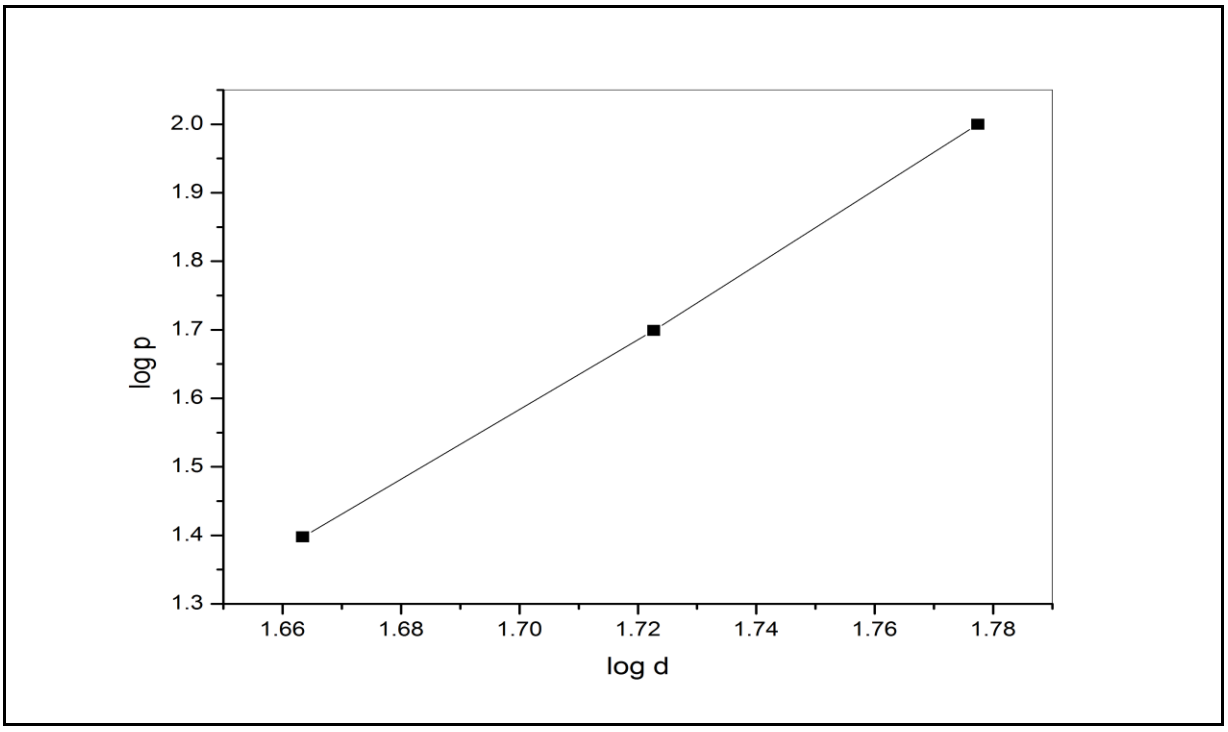

Fig.7 Meyer's plot of BGBDC single crystal

According to Meyer's law, the relation connecting the applied load $P = kd^n$, where n is the Meyer's index or work hardening exponent and k is the constant for a given material. After careful observations on various materials, Onitsch [20] and Hanneman [21] pointed out that the value of n lies between 1 and 1.6 for hard materials and it is more than 1.6 for soft material. The plot of log P against log d given in Fig. 7 is a straight line. The work hardening coefficient (n) is calculated from Fig. 7, the slope of log P versus log d and is estimated to be 5. Thus the BGBDC comes under the soft material category.

3.6 Dielectric studies

The dielectric constant and dielectric loss of the BGBDC crystal was studied at various temperatures (32, 50, 75 and 100 °C) using a HIOKI 3532 LCR HITESTER instrument in the frequency region 50 Hz to 200 KHz. Cut and polished transparent good quality single crystal of dimension 3mm × 2mm × 1mm was used. Silver paste was applied on the opposite faces of the sample. A two terminal copper electrode was used as sample holder and the sample was held between electrodes. The temperature of the sample was controlled and measured using a thermocouple. Thermocouple was fixed in the vicinity of lower electrode to measure the temperature of the sample. In this way a parallel plate capacitor was formed. The capacitance and D value of the sample was measured by varying the frequency and temperature. The dielectric constant (ε_r) was estimated at the temperature 32, 50, 75 and 100 °C by using the formula $\varepsilon_r = Cd/(\varepsilon_o A)$, where C is the capacitance of the crystal, d is the thickness of the crystal, A is the cross sectional area of the flat surface of the crystal and ε_o is the constant of permittivity of free space. Fig. 8 shows the plot of dielectric constant versus frequency. The dielectric constant is high in the lower frequency region and then it decreases with the applied frequency for all temperatures. The very high value of dielectric constant at low frequencies may be due to the presence of all four polarizations, namely space charge, orientation, electronic and ionic polarization and it is a low value at higher frequencies, which may be due to the loss of significance of this polarization gradually.

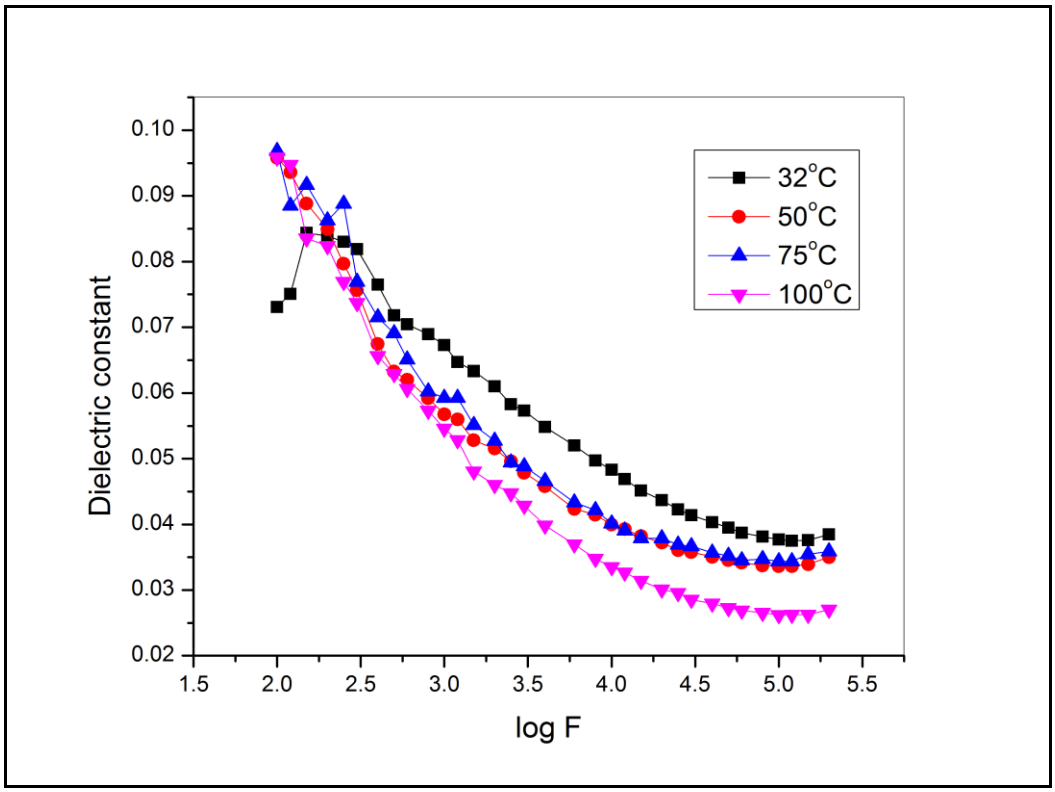

Fig. 8 Variation of dielectric constant with frequency

From the plot, it is also observed that dielectric constant increases with increase in temperature. This is attributed to the presence of space charge polarization near the grain boundary interfaces which depends on the purity and perfection of the sample [22]. The variation of dielectric loss with frequency is shown in Fig. 9. It is observed that the dielectric loss decreases with increasing frequency. The characteristic low dielectric loss with higher frequency for a given sample suggest that the sample possesses enhanced optical quality with lesser defects and this parameter is of vital important role for the fabrication of devices [23].

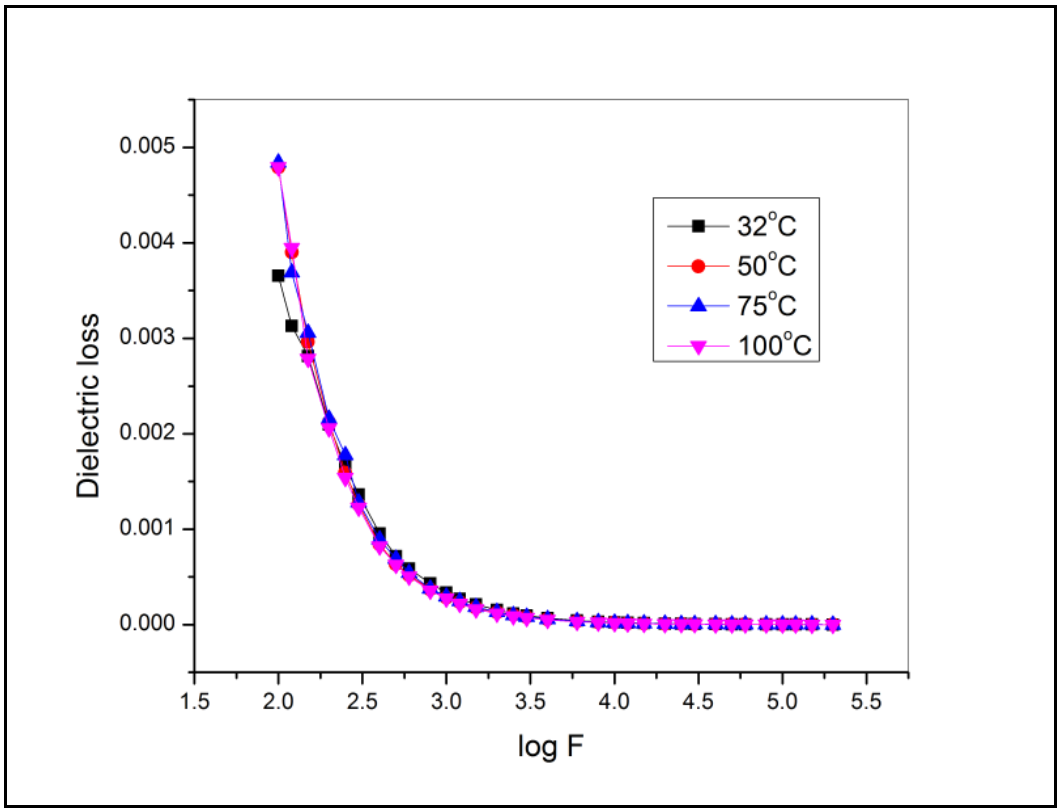

Fig. 9 Variation of dielectric loss with frequency

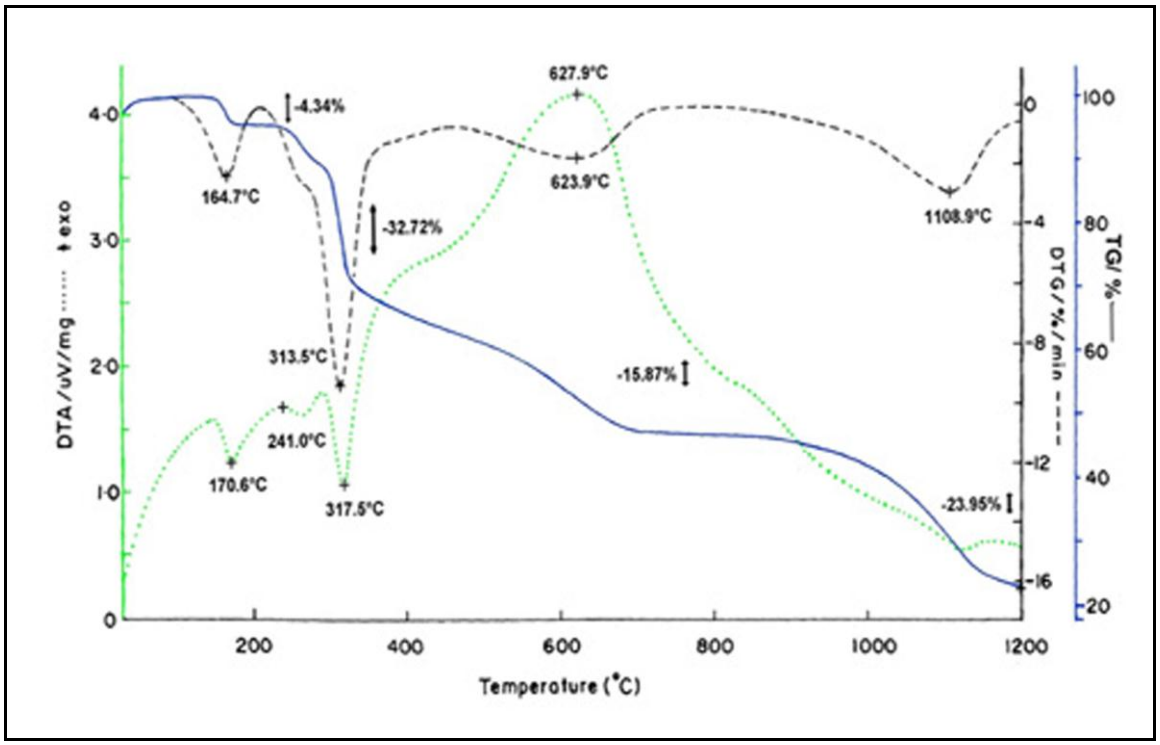

Fig. 10 TG/DTG and DTA spectrum of BGBDC crystal

3.7 Thermal analysis

The thermogravimetric analysis (TGA) and differential thermal analysis (DTA) of BGBDC were carried out between 25 °C and 1200 °C at a heating rate of 1 °C/min by employing Perkin Elmer US TGA 7 analyzer. The experiment was performed in nitrogen gas atmosphere. Four weight losses occurred in the TGA

curve and the recorded TGA and DTA curve are shown in Fig. 10. The first weight loss is attributed to the decomposition of one water molecules (4.34 %). The second and third step of weight loss indicates the decomposition of two glycine molecules (48.59 %). The final step of weight loss is assigned to the decomposition of another $BaCl_2$ molecule (23.95 %). The DTA trace indicates a weak endothermic starting at about 170.6 °C that may be assigned to the dehydration of one water molecule. A very small defused peak appears at 241 °C and can be neglected. The fourth endothermic is observed at 627.9 °C and corresponds to the loss of barium chloride molecules.

3.8 Z – Scan studies

In 1989, Sheik – Bahae et al. [24] have reported a method, the Z – Scan technique for the determination of third order nonlinear refractive index (n_2) and nonlinear absorption coefficient (β) simultaneously. In this technique, a polarized Gaussian laser beam propagating in the Z – direction, is focused to a narrow waist. The sample is moved along the Z - direction and the transmitted intensity is measured through finite aperture in the far field as a function of the sample position Z, measured with respect to the focal plane. As the sample moves through the beam focus (at Z = 0), self – focusing or defocusing modifies the wave front phase, thereby modifying the detected beam intensity. The schematic setup of the Z – Scan technique is depicted in Fig. 11.

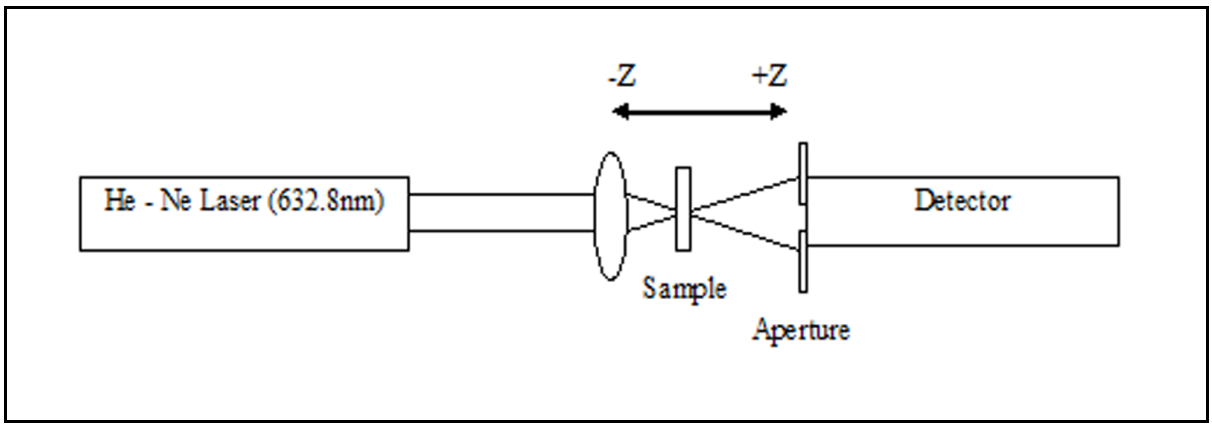

Fig. 11 Experimental setup of Z – scan technique

The third order nonlinear refractive index (n_2) and the nonlinear absorption coefficient (β) of grown BGBDC crystal was calculated by using Z – scan technique with 20 mW and the wavelength of 632.8 nm and focused by a lens of 12 cm focal length. The transmitted beam through an aperture placed in the far field was measured using photodetector with a digital power meter. In an open aperture method, a lens replaces the aperture to collect the entire laser beam transmitted through the sample. The sample causes an additional focusing and defocusing, depending on whether nonlinear refraction is positive or negative. The sensitivity to nonlinear refraction is entirely due to the aperture and the removal of aperture completely eliminates the effect. The enhanced transmission near the focus is suggestive of the saturation of the absorption at a high intensity. Absorption saturation in the sample enhances the peak and decreases the valley in the closed aperture Z – scan. The defocusing effect is produced due to the thermal conductivity resulting from the absorption of radiation 632.8 nm. A spatial distribution of the temperature in the crystal is produced due to the absorption of focused beam propagating through the absorbing sample medium. Hence a spatial variation of the refractive index is produced, which acts as a thermal lens resulting in the phase distortion of the propagating beam (Fig. 12a). The difference between the transmittance peak and valley transmission (ΔT_{p-v}) can be written in terms of the on – axis phase shift at the focus.

$$\Delta\phi = \frac{\Delta T_{p-v}}{0.406(1-S)^{0.25}} \qquad (1)$$

Where $\Delta\phi$ is the axis phase shift at the focus, S is the linear transmittance aperture and it was calculated using the relation,

$$S = 1 - \exp\left(\frac{-2r_a^2}{\omega_a^2}\right) \quad (2)$$

Where r_a is the radius of aperture and ω_a is the beam radius at the aperture. The nonlinear refractive index (n_2) was calculated using the relation [25]

$$n_2 = \frac{\Delta\phi}{kI_o L_{eff}} \quad (3)$$

Where k is the wave number ($k = 2\pi/\lambda$), I_o is the intensity of the laser beam at the focus (Z = 0).

$$L_{eff} = \frac{1 - \exp(-\alpha L)}{\alpha} \quad (4)$$

Where L_{eff} is the effective thickness of the sample, α is the linear absorption coefficient of the sample and L is the thickness of the sample. The nonlinear absorption coefficient (β) is estimated from the open aperture Z – scan data (Fig. 12b).

$$\beta = \frac{2\sqrt{2}\Delta T}{I_o L_{eff}} \quad (5)$$

Where ΔT is one peak value at the open aperture Z – scan curve. The value of β will be negative for saturated absorption and positive for two photon absorption. The real and imaginary part of the third order nonlinear optical susceptibility ($\chi^{(3)}$) were estimated using [26].

$$\mathrm{Re}\,\chi^{(3)} = \frac{10^{-4}\varepsilon_o c^2 n_o^2 n_2}{\pi}(cm^2/W) \quad (6)$$

$$\mathrm{Im}\,\chi^{(3)} = \frac{10^{-2}\varepsilon_o c^2 n_o^2 \lambda\beta}{4\pi^2}(cm^2/W) \quad (7)$$

Where ε_0 is the vacuum permittivity, c is the velocity of light in vacuum, n_0 is the linear refractive index of the sample and λ is the wavelength of laser beam. The third order nonlinear optical susceptibility was calculated using the relation

$$\chi^{(3)} = \sqrt{(\mathrm{Re}\,\chi^{(3)})^2 + (\mathrm{Im}\,\chi^{(3)})^2} \quad (8)$$

Table 2 Parameters measured in Z – scan experiment.

Laser beam wavelength (λ)	632.8 nm
Lens focal length (f)	12 cm
Optical path distance (Z)	115 cm
Spot – size diameter in front of the aperture (ω_a)	1 cm
Aperture radius ($r_{a)}$	4 mm
Effective thickness (L_{eff})	0.99 mm
Nonlinear refractive index (n_2)	1.60637×10^{-10} m^2/W
Nonlinear absorption coefficient (β)	0.77645×10^{-3} m/W
Third order nonlinear susceptibility ($\chi^{(3)}$)	3.17434×10^{-6} esu

Table 2 shows the experimental details and the values obtained from the Z - scan measurement for BGBDC. Due to excellent nonlinear response, BGBDC can be a promising material for nonlinear optical device fabrication.

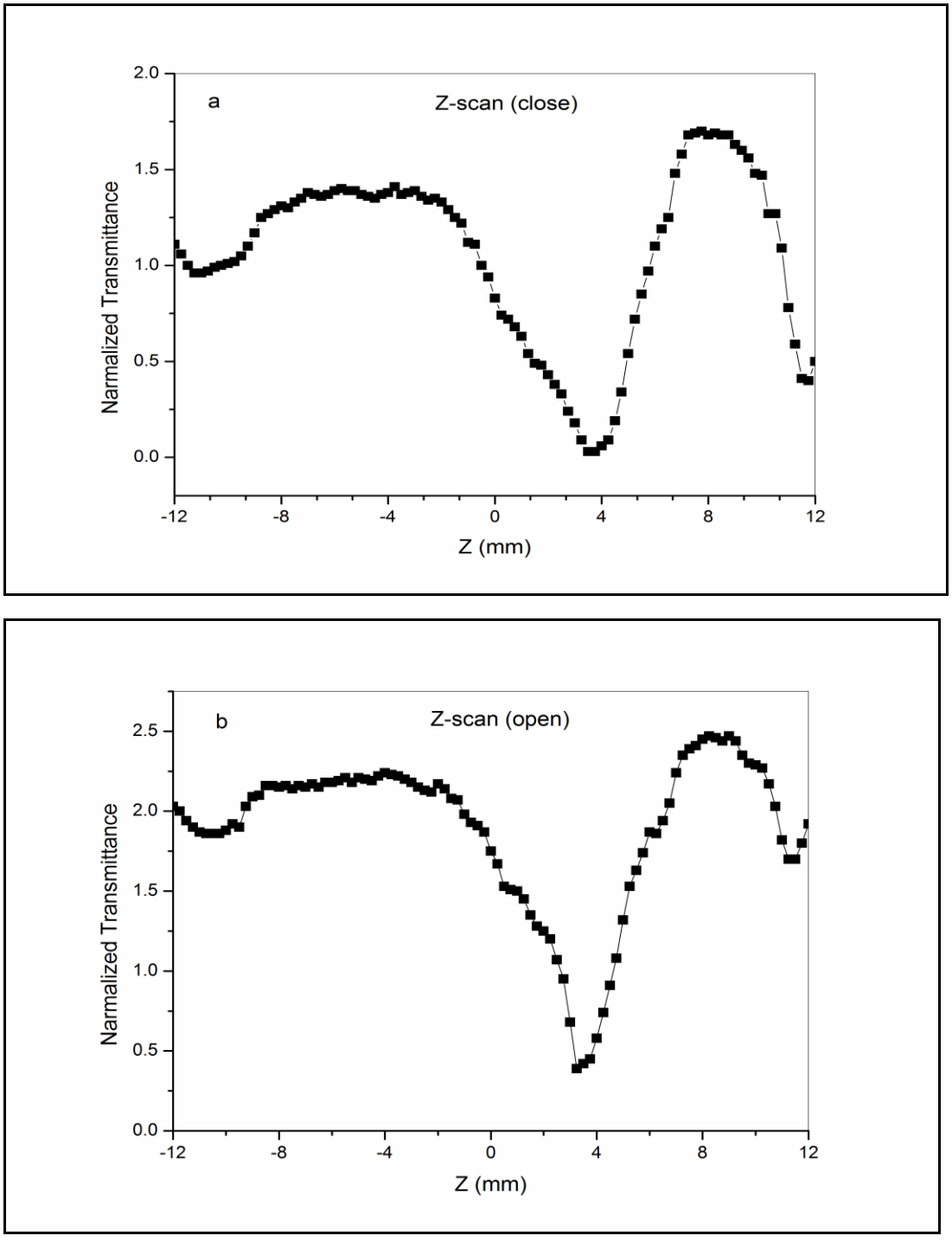

Fig.12 (a) Z – scan (close) spectrum of BGBDC and (b) Z – scan (open) spectrum of BGBDC.

4. Conclusions

Single crystals of bisglycine barium dichloride (BGBDC) were successfully grown from solution growth technique at room temperature. Solubility of BGBDC was determined at different temperatures and BGBDC exhibits of its positive temperature coefficient of solubility. The unit cell parameters were determined by single crystal X – ray diffraction analysis and BGBDC crystal belongs to orthorhombic system. Presences of various functional groups were confirmed by FTIR spectral analysis. The UV – Vis – NIR transmittance

spectrum shows that the material exhibits no absorption in the complete UV – Vis – NIR region (220 – 1100 nm). The Vicker's microhardness values increases with increasing load and the crystal experiences cracks for loads above 100 g. The variations in dielectric constant and dielectric loss were studied with varying frequency at different temperatures. TGA/DTA analysis shows that the BGBDC crystals are thermally stable up to 164 °C. The nonlinear optical refractive index $n_2 = 1.60637 \times 10^{-10}$ m^2/W, nonlinear absorption coefficient $\beta = 0.77645 \times 10^{-3}$ m/W and third order nonlinear optical susceptibility $\chi^{(3)} = 3.17434 \times 10^{-6}$ esu were calculated by Z – scan technique.

References

1. Prasad PN, Williams DJ (1991) Introduction to Nonlinear Optical Effects in Molecules and Polymers. John Wiley, New York.
2. Nalwa HS, Miyata S (1997) Nonlinear Optics of Organic Molecules and Polymers. CRC Press, New York.
3. Pal T, Kar T, Bocelli G, Rigi L (2003) Cryst Growth Des 3: 13 - 16.
4. Albrecht G, Corey RB (1939) J Am Chem Soc 61: 1087.
5. Iitaka Y (1958) Acta Crystallogr 11: 224 - 225.
6. Morrison RT, Boyd RN (1992) Organic Chemistry. 6th edition, Prentice Hall Englewood Cliffs, NJ.
7. Pepinsky R, Okaya Y, Eastman DP, Mitsui T (1957) Phys Rev 107: 1538 – 1539.
8. Pepinsky R, Vedam K, Okaya Y (1958) Phys Rev 110: 1309 – 1311.
9. Matrino D, Passeggi M, Calvo R, Nascimento O (1996) Physica B: Condensed Matter 225: 63 – 75.
10. Dacko S, Czapla Z, Baran J, Drozd M (1996) Physics Letters A 223: 217 – 220.
11. Balashova EV, Lemanov VV, Pankova GA (2001) Phys. Solid State 43: 1328 – 1335.
12. Cherouana A, Benali-Cherif N, Bendjeddou L, Merazig H (2002) Acta Cryst E58: o1351 – o1353.
13. Ambujam K, Rajarajan K, Selvakumar S, Madhavan J, Mohamed G, Sagayaraj P (2007) Optical Materials 29: 657 – 662.
14. Balakrishnan T, Ramamurthi K (2006) Cryst Res Technol 41: 1184 – 1188.
15. Michel Fleck (2008) Z Kristallogr 223: 222 – 232.
16. Narayanan P, Venkataraman S (1975) Z Kristallogr 142: 52 – 81.
17. Thomas joseph Prakash J, Vijayan N, Kumararaman S (2008) Spectrochimica Acta Part A 71: 1250 – 1252.
18. Senthil Pandian M, Ramasamy P (2008) J Crystal Growth 310: 2563 – 2568.
19. Senthil Pandian M, Ramasamy P (2009) J Crystal Growth 311: 944 – 947.
20. Onitsch EM (1947) Mikroscopia 2: 131 - 134.
21. Hanneman M (1941) Metall Manch 23: 135 - 140.
22. Smith CP (1965) Dielectric Behaviour and Structure. McGraw – Hill, New York.
23. Balarew C, Duhlew RJ (1984) J Solid State Chem 55: 1 – 6.
24. Sheik – Bahae M, Said AA, Tai –Huei Wei, David J, Hagan EM, Van Stryland (1990) IEEE J Quantum Electron 26: 760 - 769.
25. Sheik – Bahae M, Said AA, Van Stryland EM (1989) Opt Lett 14: 955 – 957.
26. Dhanaraj PV, Rajesh NP, Kalyana Sundar J, Natarajan S, Vinitha G (2011) Mater Chem Phys 129: 457 – 463.

*****